

# SPACECRAFT WAKES IN THE SOLAR WIND

Anders I. ERIKSSON (1), Yuri KHOTYAINITSEV (1) and Per-Arne LINDQVIST (2)

(1) Swedish Institute of Space Physics, Uppsala, Sweden

(2) Space and Plasma Physics, School of Electrical Engineering, Royal Institute of Technology, Stockholm, Sweden

The solar wind flow creates a wake behind any spacecraft immersed in it. We study the properties of this wake using the spherical electrostatic probes of the Electric Fields and Waves (EFW) instruments on the Cluster satellites. The satellites spin in a plane inclined only a few degrees with respect to the ecliptic plane. The solar wind is often close to this plane, so each probe (44 m away from the spin axis) passes through the wake once every spin period (around 4 s), thereby sampling a cut of the wake electrostatic potential structure. The signature of the wake is clearly seen in the data as a pulse with an amplitude typically of a few tenths of a volt. We present statistics of the wake signatures as well as detailed examples, compare to solar wind parameters, and show a method to remove the wake signature from the electric field measurements.

## 1. INTRODUCTION

A wake necessarily forms behind any object in a supersonic flow of plasma or neutral gas. In space plasmas, spacecraft usually encounter mesosonic flows, i.e. flows which are supersonic with respect to the ion thermal speed, but subsonic with respect to the electron thermal speed. The result is that the wake charges negatively until the potential in the wake is sufficiently negative to prohibit further accumulation of electrons.

A substantial literature on spacecraft wake formation has accumulated over the years. The basic theoretical understanding was summarized already by Al'pert et al. [1] and Gurevich et al. [2] in the sixties, though significant extensions have also been achieved in later times, particularly regarding laboratory work, on-orbit investigations and numerical simulations. Most work have concentrated on wakes behind objects at negative potentials with respect to the plasma, as is relevant for satellites in the ionosphere. There are several reasons for this: wakes are most conspicuous in ionospheric data, where all spacecraft move in the mesosonic regime almost always; in the ionosphere, spacecraft are larger than the Debye length, giving large wakes charged to potentials of order  $KT_e/e$ ; wakes in the ionosphere have influence on the charging of spacecraft and thus are of interest for spacecraft design and operations; and most satellites, particularly the bulk of all manned spacecraft, operate in the ionosphere.

Though it was realized early [3] that spacecraft in the solar wind would generally be positive, wake formation around positive spacecraft potentials has therefore received little attention until recently. There are a few exceptions, including early linearized analytical models [4, 5] of uncertain validity [1, p. 91], laboratory investigations [6] and some numerical work, old [7, 8] as well as more recent [9, 10, 11, 12, 13]. Nevertheless, for satellites doing scientific measurements in less dense regions, like the magnetosphere above an altitude of a few thousand kilometers and all of the solar wind, the case of wakes around positive spacecrafts is important. Mesosonic flows occur in at least two regions above the ionosphere. The polar wind is a mesosonic outflow from the Earth into the lobes of the magnetotail. Because the polar wind ion flow energy  $mu^2/2$  (which may be below or around 10 eV) is not sufficient to overcome the spacecraft potential  $V_S$ , which can be several tens of volts positive because of the low density in the lobes [14], the ions scatter on the potential structure around the spacecraft, so that wakes forming behind spacecraft in the polar wind can have dimensions much larger than the spacecraft size. The exploration of this topic is very recent [15, 16], as reported elsewhere in the present volume [17].

The other region above the ionosphere where mesosonic flows are commonly encountered is the solar wind.

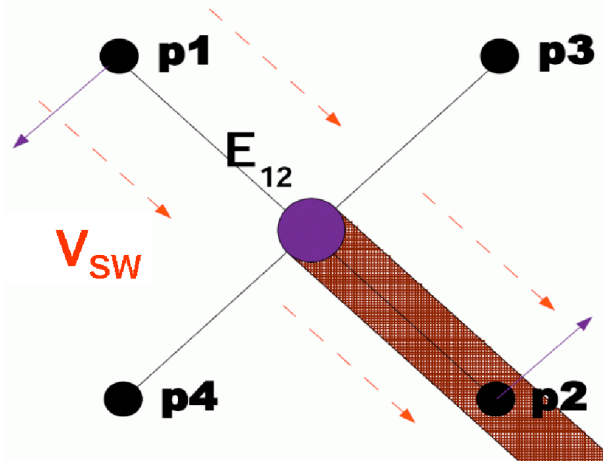


Fig. 1. Sketch of Cluster and EFW probe geometry, with the wake forming behind the spacecraft. In reality, the wake will spread out at an angle related to the flow Mach number.

While a satellite in the solar wind develops a positive potential  $V_S$  of up to or around 10 V due to the low plasma density, the ion flow kinetic energy  $mu^2/2$  of around 1 keV will always be sufficient for letting the ions reach the spacecraft. The wake forming in such a situation will thus be narrow, but it will, as we will see, still be detectable. We use the term *narrow wake* for this wake, forming when  $mu^2/2 > eV_S$ , to discriminate from the much broader *extended wake* discussed in [17] that forms when  $mu^2/2 < eV_S$ .

We base this study on data from the Electric Fields and Waves (EFW) instruments on ESA's four Cluster satellites. Each EFW instrument uses four spherical sensors at the tip of wire booms arranged as an orthogonal cross in the satellite spin plane. The distance between opposing probes is 88 m, and the spin period is close to 4 s. Further instrument information is provided in references [18] and [19], the latter also giving a thorough introduction to the measurement technique. Figure 1 shows a sketch of wake generation behind Cluster and its detection by EFW. The Cluster satellites [20] were launched by ESA in the summer 2000 into a polar orbit of roughly  $4 \times 20 R_E$  and have by now acquired detailed four-point measurements in the terrestrial magnetosphere and the adjacent solar wind for the declining half of one solar cycle. Apart from EFW data, we will also use supporting data from the Cluster Ion Spectrometers (CIS, [21]), particularly the Hot Ion Analyzer (HIA) instruments in this paper.

## 2. EXAMPLE DATA

Figure 2 shows an example of a narrow wake, acquired by the EFW instrument on Cluster 3 (that is, number 3 of the four Cluster spacecraft) in the solar wind. The data is the electric field measurement (probe voltage difference) from two opposing EFW probes during 12 s, or three spacecraft spin periods, in the spinning spacecraft frame of reference. As expected, the effect of the spacecraft spin is obvious in this rotating frame of reference, modulating the electric field with a sinusoid of period close to 4 s. The blue curve shows the original data. Twice every spin, a narrow ( $< 0.5$  s) pulse can be clearly seen in the data, positive once and negative once per spin. The pulse pattern is very repetitive, and positive and negative pulses are approximate mirror images of each other.

The artificial nature of these pulses is very clear, not least from the perfect repetition at spacecraft spin frequency. At first glance, the pulses may be thought to those seen in electric field data from the EXOS-D/Akebono satellite by Amano et al. [22]. However, we will show that any similarities are incidental, and the actual mechanisms behind the pulse-like signatures in Cluster and Akebono electric field data are very different. In the case of Akebono, which is always inside the magnetosphere with an apogee of 10 500 km, the reason presented by Amano et al. is that photoelectrons from the spacecraft, whose potential is a few volts positive, reach the probes when the wire booms are aligned to the ambient magnetic field. The Akebono electric

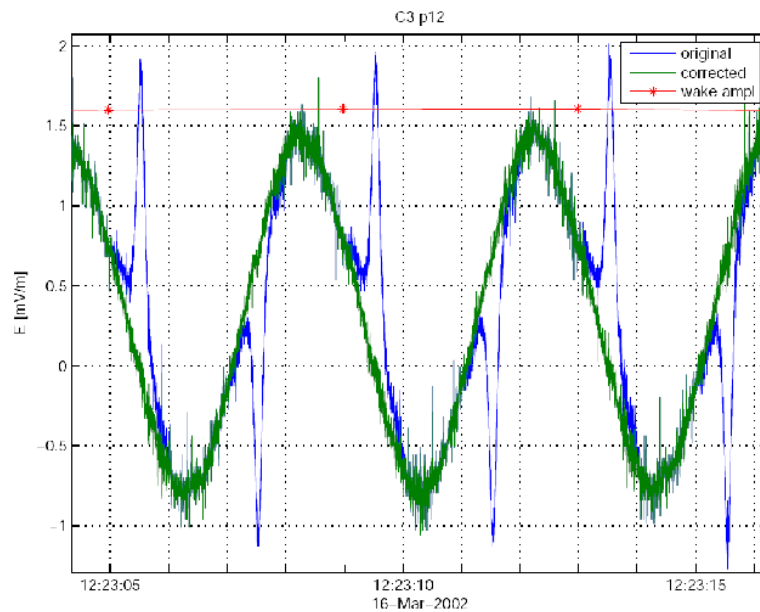


Fig. 2. Example of solar wind wake signature in Cluster EFW data. The blue curve is the original raw data, while the green curve shows the data after wake removal (Section 3). The red stars, bound together by the red curve, shows the wake amplitude determined in the removal process, once for each spacecraft spin period.

field results are consistent with the previous investigations of Langmuir probe data from the Viking satellite by Hilgers et al. [23, 24, 25] in an orbit similar to Akebono's, which were also explained by a similar mechanism. The features we are studying are quite different, as will be discussed in Section 4.1 (item 9).

### 3. WAKE IDENTIFICATION AND REMOVAL

The wake signature is interesting in itself, and also for what it can reveal about the solar wind plasma. However, it also constitutes a major contamination of the measurement of the naturally occurring electric field. For example, any spectrum of the electric field will show strong spin harmonics because of the wake. It is therefore of interest to produce cleaned electric field data, particularly for the Cluster Active Archive [26], which is becoming a major repository of validated data from all Cluster instruments and the major source of Cluster data for the scientific community.

The wake signature depends on the solar wind flow properties and is therefore usually slowly changing on the Cluster spin timescale of 4 s. Exceptions to this of course exist, particularly at boundaries, but for the bulk of the solar wind data the proposition holds true. This enables us to construct a "find and fix" algorithm based on determining the wake for a given spin as the average of the wakes for this and adjacent spins. The algorithm have to take care of a lot of special cases related to data gaps, missing data, interference from the WHISPER sounder and so on, but its general features are as follows (see also Figure 3):

- 1) Organize the data per spin.
- 2) Resample the data from the original time series (at 25 or 450 samples/s) to get uniform  $1^\circ$  resolution.
- 3) For each spin, form a weighted average of the data from that spin and its four closest neighbours. We use weights [0.1, 0.25, 0.3, 0.25, 0.1]. The wake signature, which is very repetitive (Figure 2), will not be much changed by this, while unrelated time variations from wave activity will be damped.
- 4) Calculate the second derivative of the averaged data. This will exaggerate the wake signature at the expense of the background sinusoidal spin signature of the natural electric field in the plasma.

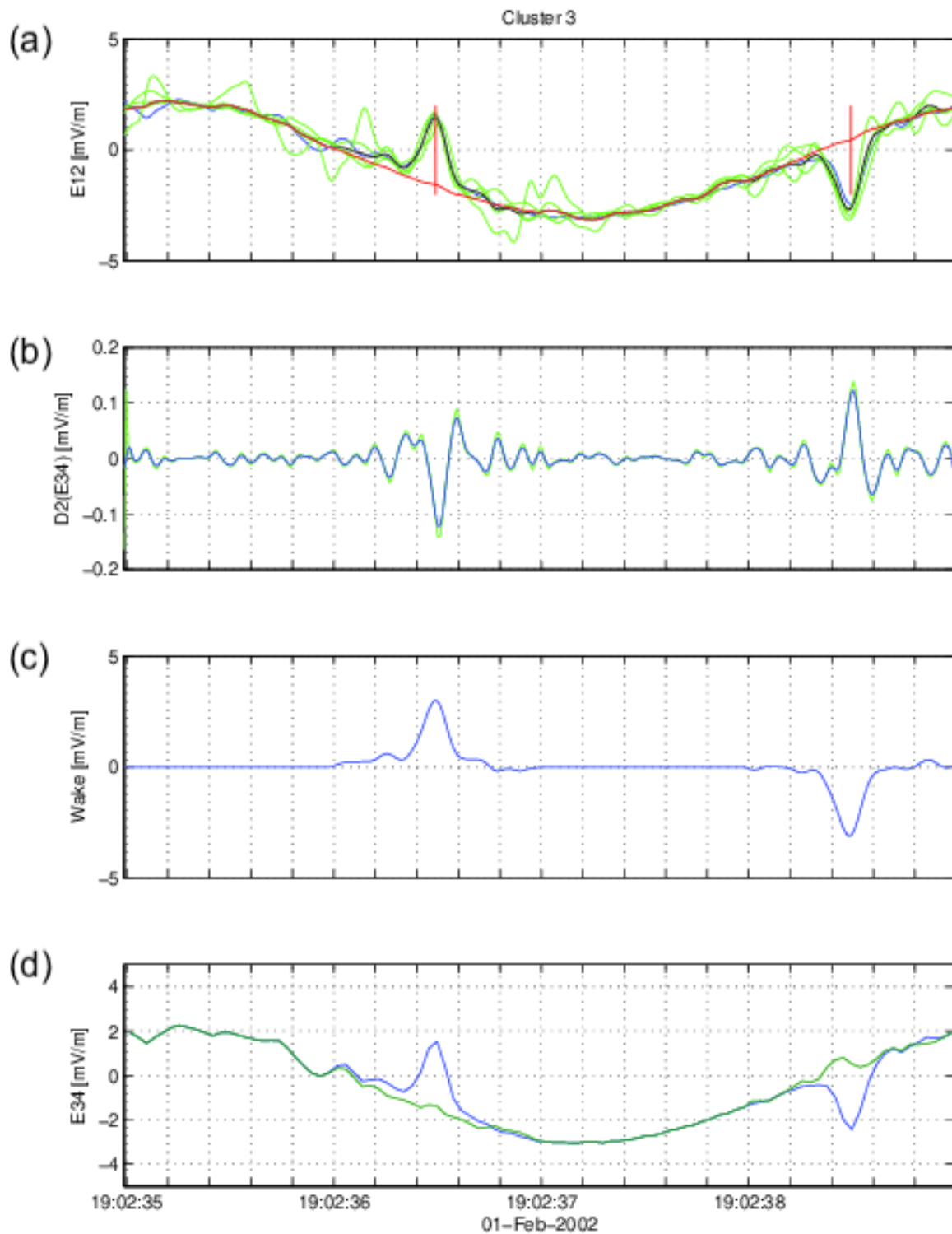


Fig. 3. An example of wake identification and removal from one spin of EFW data from Cluster 3. (a) The electric field data for the spin under study are plotted in black, with the four adjacent spins given in green. (b) The second derivative of the weighted average of the five spin periods of data above. (c) After smoothing of the second derivative, it is integrated twice to give a wake time series. This is set to zero far from the wake centre. The amplitude and width of the wake are determined from these data. (d) The original time series (blue) and the corrected data (green).

- 5) Apply a smoothing filter (we use 7-point moving average) to minimize the effect of wave noise, which has been boosted by the differentiation.
- 6) Find candidates for wake centre positions by looking for maxima of the magnitude of the second derivative.
- 7) Integrate twice to recover a smoothed version of the original time series.
- 8) Take the average of the two wakes found in the spin (account for the sign) to get an average wake form for this spin.
- 9) Set the data far from the candidate wake centre positions in this time series to zero, so that only data close to the wake will be affected by the eventual wake removal.
- 10) Apply restrictions on allowed angle with respect to the solar direction, amplitude, shape and width of the signature that it must meet to qualify as a wake.
- 11) Remove the wake signature from the original time series of the spin under study.
- 12) Consider this to be a preliminary wake estimation and cleaning, that may be influenced by the fundamental natural electric field signal at the spin frequency, particularly if the wake occurs close to an extremum in the spin frequency electric field. To minimize such errors, we fit a sinusoidal signal at the spin frequency to the preliminary cleaned data, remove this from the original data, and perform steps 1–11 again on data that thus have most of the original spin electric field removed.
- 13) Thus we arrive at a final wake estimation which we subtract from the original data to create a final cleaned electric field signal. Save characteristic data for the wake: spin phase angle  $\phi$ , full width at half maximum (FWHM)  $w$ , and maximum amplitude  $A$ .
- 14) Repeat procedure for next spin.

That this algorithm is quite effective is illustrated by the data in Figure 4. The upper panel shows 20 minutes of full resolution EFW electric field data, in the spinning spacecraft frame, acquired in the solar wind and bow shock regions. The wake amplitude is very stable for more than 10 minutes, and varies reasonably slowly even rather close to the activity associated with the bow shock, which we see from 12:32 to 12:36. A detail of these data is shown in the lower panel. It can be seen that the wake signature appears in the data when exiting the turbulent region around 12:35:22 – it may indeed be present inside that region as well, but is hard to discern even for the human eye in this dynamic region. The wake is easily spotted from 12:35:24 onward, but it clearly takes a few spins before it stabilizes sufficiently for the wake algorithm to be able to correctly identify the wake pulse in the data and correct for it. However, it partially alleviates the wake, and hence improves the quality of any spectrum calculated from these data, even though the fix is not perfect. But already from 12:35:40 the fix is very good, and at the end (and for the following hours) it appears almost perfect to the human eye.

This perfection is of course an illusion. Removing the wake, by however clever an algorithm, will always be a manipulation of the data. Any real plasma signals on the same time scale will also be removed in the process, and natural features from surrounding spins may be introduced by the averaging. Nevertheless, it is clear that removing the wake vastly increases the usefulness of the data, as the major artificial signal (which sometimes can dominate the time series) is removed.

#### 4. WAKE STATISTICS

The algorithm described in Section 3 collects data on some of three primary characteristics of the wake: its position in the spin plane  $\phi$ , its amplitude  $A$  and its width, quantified as the FWHM value,  $w$ . If the shape of the wake was Gaussian, these parameters would be sufficient to fully describe it. As the algorithm is used in the production of EFW data for the Cluster Active Archive, statistics pile up quickly. In the present study, we

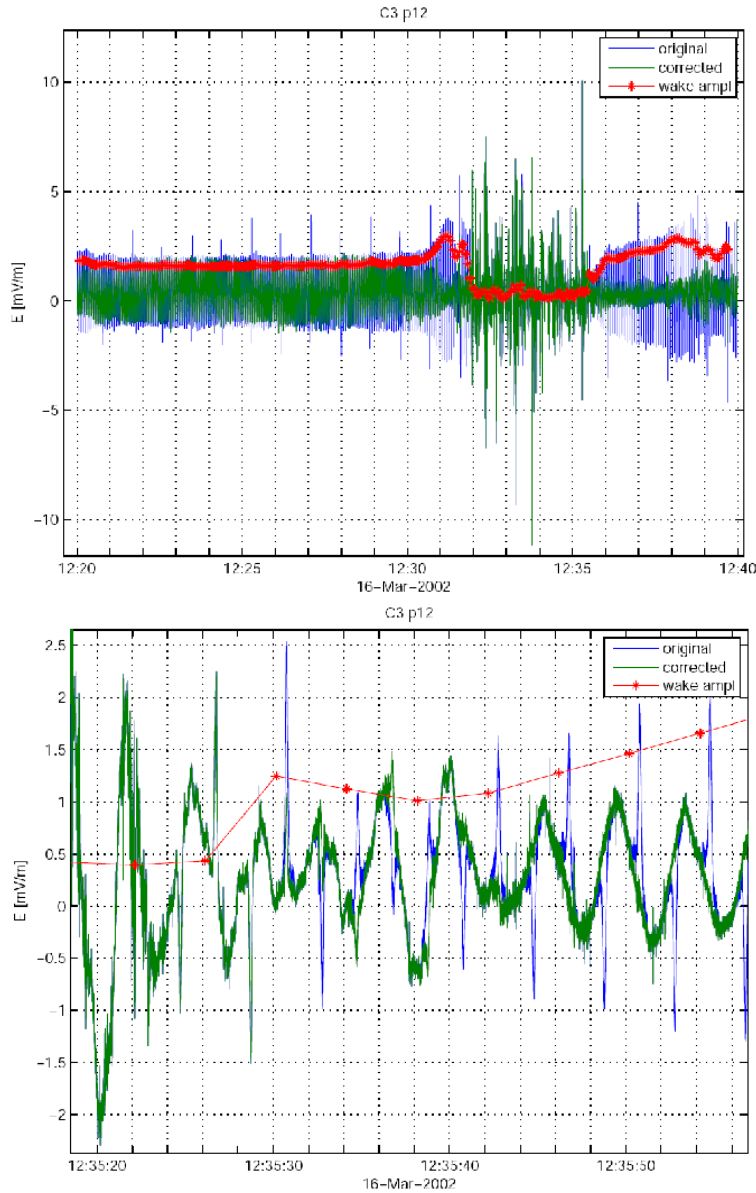


Fig. 4. Full resolution raw (blue) and wake corrected (green) electric field data from EFW probes 1 and 2 on Cluster 3. The red curve denotes the wake amplitude. The lower panel is a zoom in to a detail of the upper panel.

limit ourselves to data from Cluster spacecraft 3, and restrict ourselves to the time period February-April 2003. During this period, 1,170,617 wakes were identified and corrected for on Cluster 3, forming a decent statistical sample.

#### 4.1 1D distributions

Figure 5 shows the observed distributions of the wake parameters and some complimentary data. The CIS data used in this study are prime parameters from the Cluster Science Data System, CSDS [27]. We comment the histograms one by one:

- 1)  $V_{ps}$ , the probe-to-spacecraft potential, can be viewed as a quasi-logarithmical density proxy [14, 28], but should also be important for the wake because it to a large extent determines the electrostatic environment around the spacecraft. The distribution seen is typical for the solar wind [29].
- 2) CIS  $n$ , the plasma density from the CIS HIA detector, shows a distribution typical for solar wind values.

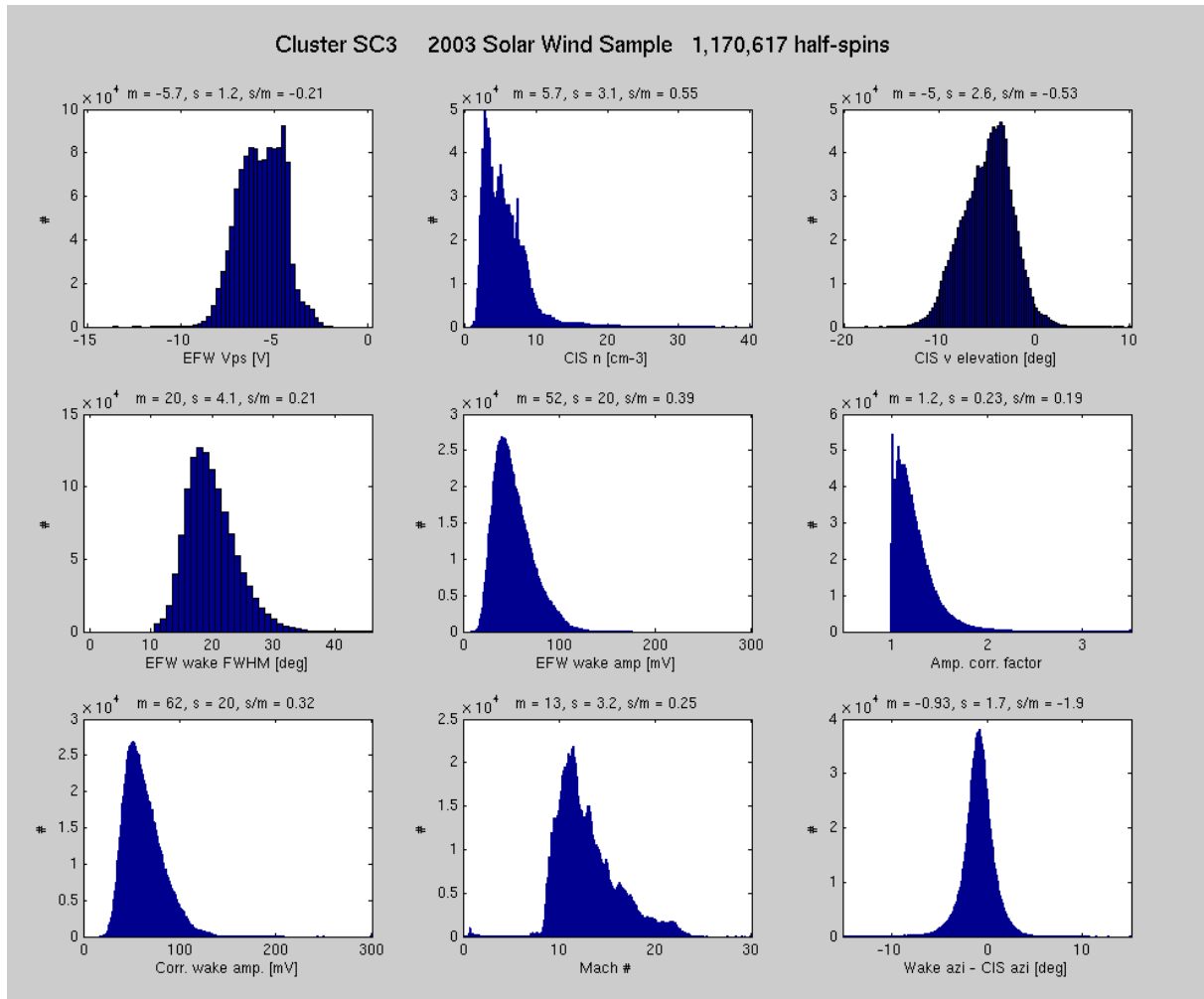


Fig. 5. Statistical distributions of wake parameters and related data for the statistical sample used in this paper. On top of each panel is given the mean  $m$ , standard deviation  $s$  and normalized spread  $s/m$  for the plotted variable.

- 3) CIS  $v$  elevation is the angle of the flow to the spin plane as observed by the CIS HIA detector. Because the spin axis is inclined at typically  $5\text{--}6^\circ$  with respect to the ecliptic plane, the peak is offset from zero, and has a mean of  $5.0^\circ$ . The distribution shows a clear skewness: we have not investigated the reason for this, or if this is typical for solar wind conditions at other times.
- 4) The EFW wake FWHM value,  $w$ , has a mean value of  $20^\circ$ . One should note that this estimate may be biased because we have discarded all wakes with width below  $10^\circ$ , as such cannot be reliably determined with the predominating 25 Hz sampling rate of EFW. Nevertheless, preliminary checks of data acquired at 450 samples/s do not show any big difference from this distribution, so the number of wakes discarded because of low width is small: the drop below  $18^\circ$  appears to be real.
- 5) The EFW wake amplitude,  $A$ , shows a mean of 52 mV, and a smooth distribution. Very weak wakes may not be detected, and hence the lower part of this distribution could be uncertain.
- 6) The amplitude correction factor is discussed in Section 4.2.
- 7) The corrected wake amplitude is discussed in Section 4.2.
- 8) The Mach number is here defined as the ratio of the CIS ion flow speed to the thermal ion velocity, defined as  $\sqrt{KT_{i\perp}/m_p}$ , where  $KT_{i\perp}$  is the perpendicular temperature moment from CIS HIA and  $m_p$

is the proton mass.

- 9) The difference between the wake direction in the spin plane seen by EFW and the solar wind flow direction shows a very narrow distribution. The two measurements agree to  $-0.9^\circ$  with a standard deviation of  $1.7^\circ$ . While the mean value will be discussed in Section 4.3, we may note that the standard deviation is as small as it could ever be, as the typical EFW sampling rate of 25 samples/s corresponds to an angular resolution of  $3.6^\circ$ . This impressive agreement clearly shows that the phenomenon at hand is a velocity wake, not a magnetic effect as those studied on Viking [23] and Akebono [22] (see Section 2). In addition, a plot of the relation between magnetic field direction and wake direction (not shown) shows no correlation at all.

## 4.2 Gaussian wake modelling

One way to test our understanding of the wake data is to investigate the relation between wake amplitude, width and the flow elevation angle. As a first model, we may assume that the shape of the wake is Gaussian. This will be the case if the plasma is Maxwellian, if the electric potential in the wake is so small as to not really influence particle motion and if we are sufficiently far from the spacecraft [1, p. 25]. All these requirements are probably violated for Cluster in the solar wind, with the approximation of a "neutral wake" (no influence of wake electric fields on its structure) being the most problematic. This can also be seen in the wake signature in the bottom panel in Figure 3, which suggests that the wake deviates from a Gaussian shape at least by having a broad sheath around it. Such a structure is actually expected, with a sheath characterized by self-similar expansion surrounding a central wake core where the neutral approximation applies [30, 31].

Nevertheless, a Gaussian form is a good starting point not only for this reason, but also because its factorization properties. Assume the wake potential is of the form

$$\Phi(x, y, z) = A_0 f(z) \exp\left(-\frac{x^2 + y^2}{a^2}\right) \quad (1)$$

where  $z$  is the coordinate along the flow direction, the origin is at the centre of the spacecraft and  $a$  is related to the FWHM by

$$w = 2a\sqrt{\ln 2}. \quad (2)$$

If a probe cuts the wake through its diameter, as it would do if the flow was exactly in the spin plane, we put  $y = 0$  and the observed extremum amplitude is clearly the wake amplitude at that distance, because  $\Phi(x) = A_0 f(z) \exp(-x^2/a^2)$ . If, however, the flow is out of the spin plane so that the probe cuts the wake along a chord whose closest distance to the wake axis is  $b$ , then

$$\Phi(x) = A_0 f(z) \exp(-b^2/a^2) \exp(-x^2/a^2). \quad (3)$$

Note that the observed FWHM value is independent of  $b$ , as we derive it from a series of data with varying  $x$ . Hence, if we know that the flow direction is elevated by an angle  $b$  from the spin plane, we expect the real amplitude at distance  $z$  from the spacecraft,  $A_0 f(z)$ , to be related to the amplitude we observe,  $A = \max(\Phi(x))$ , by

$$A_0 f(z) = A \exp(b^2/a^2) \quad (4)$$

if the wake is assumed to be Gaussian in the angles. This is in fact a substantial difference from being Gaussian in the Cartesian coordinates as we saw in Section 4.1 that the wake width (FWHM) shows a mean as large as  $20^\circ$ , and can reach above  $30^\circ$  at times. Nevertheless, as the EFW probes are at constant distance  $r = 44$  m from the spacecraft, not at constant downstream coordinate  $z$ , assuming Gaussian shape in the Cartesian coordinates would mean that we had to enter some assumption on  $f(z)$ , so we here stick to the angular Gaussian as a first approximation. It therefore makes sense to correct the wake potential for the inevitable underestimate due to the probe not passing through the centre of the wake by means of Equation (4), with  $a$  calculated from the observed FWHM as in Equation (2) and  $b$  is the CIS flow elevation angle.

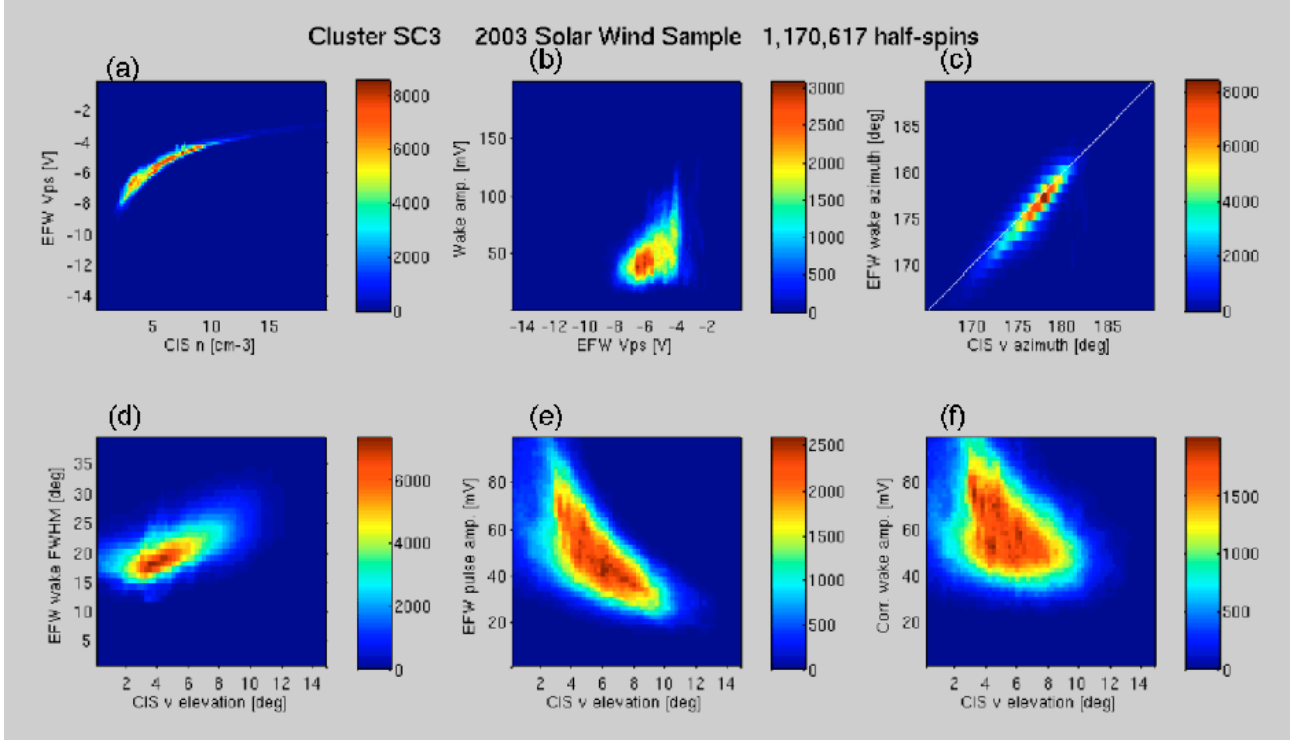


Fig. 6. Two-dimensional histograms of wake and plasma parameters. Colour scales give the number of samples in each bin.

The distribution of this amplitude correction factor,  $\exp(b^2/a^2)$ , is plotted in the right panel in the centre row of Figure 5. The distribution of the corrected amplitudes,  $A \exp(b^2/a^2)$ , is shown in the left panel of the lower row. Comparing to the uncorrected amplitude in the centre of the middle row, we find that the spread, defined as the ratio of the standard deviation  $s$  to the mean  $m$ , has decreased from 0.39 to 0.32. That the spread decreases shows that our basic understanding of the wake geometry is correct: had the amplitude, width and flow elevation not been connected by a relation like (4), the spread would not have decreased by the application of this correction factor. While this does not imply that the wake is exactly Gaussian, it demonstrates that the cause of the pulse-like signatures is a wake with a similar geometric structure.

Note that our assumption of a Gaussian wake is only used for deriving a corrected wake amplitude: the rest of this study is independent of this assumption.

### 4.3 2D distributions

To further see the correlation between the wake parameters, we present two-dimensional histograms in Figure 6. Panel (a) illustrates how the probe-to-spacecraft potential  $V_{ps}$ , which is linearly related to the spacecraft potential, depends on the plasma density as measured by CIS. This relation is further discussed elsewhere in this volume [32], and is often invoked for using  $V_{ps}$  as a density proxy [14].

Panel (b) shows the variation of wake potential amplitude with  $V_{ps}$ , and hence with density. An increasing trend can be discerned, which can be understood as an effect of the Debye length for the charging of the wake. If we remove all ions but keep all electrons in a cylindrical region of a plasma, the resulting potential will scale as

$$\Phi \sim \frac{KT_e}{e} \left( \frac{R}{\lambda_D} \right)^2 \quad (5)$$

for wake radii  $R \lesssim \lambda_D$ . Typical Debye lengths in the solar wind are 5–10 m, and the transverse size of the depleted region should not be too different from the spacecraft dimensions even as far downstream as the EFW bbom length of 44 m, so we should indeed be in this regime. Shorter Debye lengths should thus give higher wake potentials, as observed.

Panel (c) is a deeper look at the relation between the wake direction from EFW and the flow direction from CIS. While the points obviously line up nicely, there is a small but very consistent deviation from the straight line of slope one as we go away from the purely antisunward direction ( $180^\circ$ ). This means that the wake direction from EFW data is a few degrees more sunward than the flow direction from CIS. It is clear that this is the reason for the small negative mean we saw in Section 4.1, Item 9. We do not know the origin of this phenomenon. It may be due to the photoelectron cloud around the spacecraft, which is primarily controlled by the direction to the sun rather than the flow direction, influencing the wake structure, or be due to some artefact arising from the EFW or CIS measurements.

In Panel (d) of Figure 6, we find a clear deviation from what we would expect for a perfectly Gaussian wake (Section 4.2). While Equation (3) implies that the observed width  $w$  should be independent of flow elevation angle over the spin plane, Panel (d) shows that this is not the case.

Finally, Panels (e) and (f) in Figure 6 show the pulse amplitude detected by EFW. Panel (e) shows the general characteristic expected by an axially symmetric wake aligned with the flow direction: the probes on the wire boom on the spinning satellite cut a chord through the wake, and the further the chord is from the centre axis, the smaller is the pulse amplitude detected. In Panel (f), we show the result of applying the amplitude correction factor defined by Equation (4), which assumes a Gaussian wake structure. Comparing to Panel (e), we see a partial but certainly not complete removal of the dependence of the amplitude on flow elevation angle. This leads to the same conclusion as in Section 4.2: the Gaussian assumption catches some general aspects of the wake, but the detailed shape of the wake is not well described by a Gaussian.

## 5. NUMERICAL SIMULATION WITH SPIS

The data presented here makes clear the nature of the pulses in electric field data in the solar wind, and the algorithm described in Section 3 does a good job in cleaning EFW data from the influence of the wake. However, there are still reasons for further study of the solar wind wake. If we have a good theoretical model of the wake, it may be possible to use determine plasma parameters like the ion and/or electron temperatures from the wake measurements, by inversion of the model or fits to it. Such theoretical understanding will require better models than the simple Gaussian we used in Section 4.2, and would need to be compared to numerical simulations, or possibly be empirical parametrizations of results from such simulations.

In Figure 7, we show a result from a first numerical simulation using the SPIS simulation package, available at <http://www.spis.org> and described in several papers [33, 34, 35]. SPIS is a comprehensive package running on a multitude of platforms, which makes it very useful for desktop simulations like this, where only a small amount of manpower can be invested in the simulation. The simulation presented here was run on an ordinary 1.8 GHz Pentium M linux laptop computer with 1.5 GB of RAM, on which it completed within 20 hours.

The simulated plasma is typical for the solar wind: number density  $10 \text{ cm}^{-3}$ , electron temperature 10 eV, ion temperature 5 eV, and flow speed 310 km/s. The ions are all assumed to be protons. In such a plasma, the Cluster spacecrafts would usually attain a spacecraft potential of 4–5 V, as can be seen from Figure 6a. However, in this simulation we have put the spacecraft potential to zero. This makes it much simpler to extract the potential due to the space charge in the wake, as we do not have to subtract any vacuum field, and should not introduce any appreciable errors to the wake structure: the protons all arrive at energies around 500 eV, and would thus care little about a few volts of potential anyway. The electron distributions will be affected, but only very close to the spacecraft, so that any impact on the distant wake from this assumption will be negligible. We have set SPIS to use a full PIC implementation for the ions, while the electrons are assumed to be Boltzmann distributed.

The simulation region is a circular cone with its top chopped off, so it has circular cross sections at the downstream and upstream ends. The upstream circle has a radius of 13 m and is 15 m in front of the spacecraft, while the downstream boundary is 27 m in radius and is located 90 m downstream of the satellite body. The spacecraft is a circular cylinder, 1.5 m in radius and 1 m in height, centred at the origin with its axis along the

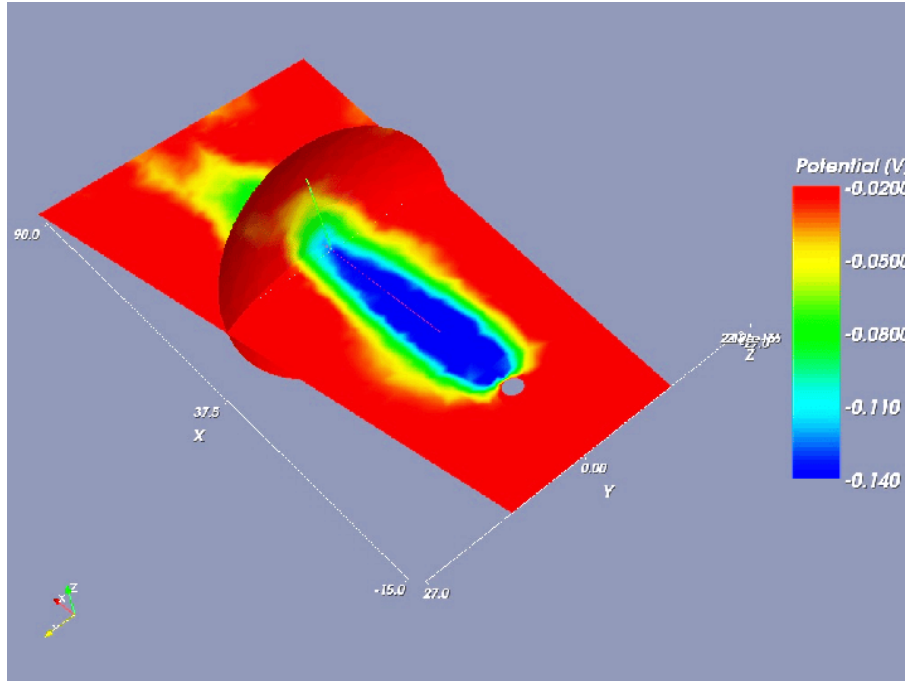


Fig. 7. Wake potential from a SPIS simulation. The solar wind flow is along the  $x$  direction, and the satellite spin axis is along  $z$ . The potential is colour coded on the  $xy$  plane and on a spherical surface with radius 44 m. The latter represents the wake region crossed by the EFW probes, at different values of  $z$  depending on the flow elevation angle over the spin plane.

$z$  axis, while the flow is in the positive  $x$  direction. The characteristic dimensions for the automatic gridding are set to 3 m on the outer boundaries and 0.5 m on the spacecraft. This resulted in a division of the simulation volume into just under 46,000 tetrahedra.

The Poisson equation is solved using an implicit scheme, and some under-relaxation is used to stabilize the plasma calculations. The total simulation time is 1 ms, selected to be roughly three times the solar wind propagation time through the simulation region. The average number of macroparticles per cell is set to 60. The number of macroparticles was 1.85 million at the start of the simulation and 2.63 million at the end. No photoelectrons or magnetic fields are included in the simulation: this is justifiable as most photoelectrons will be retained close to the spacecraft by its positive potential, and the relevant particle gyroradii in typical solar wind magnetic fields (some 5 nT) are larger than the simulation volume.

Figure 7 clearly shows a wake forming behind the satellite, charging to about -140 mV at the spherical shell at 44 m distance where the EFW probes will make their measurements. For zero flow elevation, each probe crosses the wake along the intersection of the planar and spherical surface elements in Figure 7. For nonzero flow elevations, the probe moves along the intersection of the spherical surface with a plane through the spacecraft, similar to the plane shown but turned around the  $y$  axis by the elevation angle. This wake cut may be approximated by a cut of the spherical segment at constant nonzero  $z$ . We present such cuts in Figure 8. While some general similarity with the example observation in Figure 2c is clear, a more detailed investigation of the shapes of the observed wakes as well as a larger number of simulations with refined grid resolution would be necessary for a detailed comparison. One interesting feature is the local maxima on the edges of the wake seen in the simulation. There is no obvious such structure in the example data in Figure 2c: it would be interesting to study a larger number of wake shapes to see if they turn up only in some cases, or never at all. The simulated wake amplitudes at 44 m are around 90 mV for 5° flow elevation and 50 mV for 10°. These values lay in the upper range of what we would expect from Figure 6e, but we should note that a careful comparison also will need to take into account the effect of the 10 Hz anti-aliasing filters and 25 Hz sampling frequency of the EFW instrument, which should be applied to the simulation data in order to make them fully comparable.

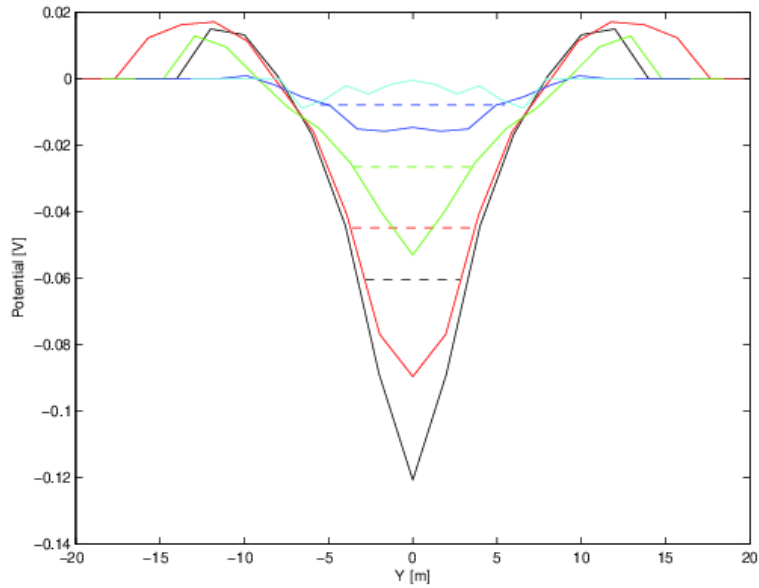


Fig. 8. Wake potential profiles 44 m downstream of the spacecraft from the SPIS simulation, obtained for different solar wind flow elevation angles above the spin plane:  $0^\circ$  (black),  $5^\circ$  (red),  $10^\circ$  (green),  $15^\circ$  (blue) and  $20^\circ$  (cyan). The half-maximum levels are indicated by dashed horizontal lines.

## 6. CONCLUSIONS

In this paper, we have described the formation of wakes behind spacecrafts in the solar wind. We have shown the signature of the wake in data from electric field measurements on the Cluster satellites, and how to separate the contribution from the wake from the natural electric field. We presented statistics of the wake based on a large sample of over 1 million wake observations, showing general consistency between expected and observed wake characteristics. We have verified the wake formation in a numerical simulation with SPIS and discussed its possible use for determining plasma parameters. Our principal results can be summarized as follows:

- 1) The Cluster electric field instrument EFW detects pulse-like signatures in the solar wind, repeated at spin frequency.
- 2) These structures are shown to be caused by a wake behind the spacecraft: they align with the flow, and their amplitude decreases as the flow elevation angle above the spin plane increases.
- 3) We have constructed an algorithm for detecting and removing the wakes from the electric field data.
- 4) The wake formation is confirmed by SPIS simulations.

## Acknowledgements

We thank the CIS team (PI Henri Rème) for the HIA particle data. We also thank the SPIS developers, the SPIS sponsor ESA and the SPINE network for creating not only the SPIS code but also a stimulating scientific and human environment around it. This study was supported by the Swedish Space Board (Cluster EFW operations and data analysis) and by ESA (the EFW part of the Cluster Active Archive).

## References

- [1] Ya. L. Al'pert, A. V. Gurevich, and L. P. Pitaevskii. *Space Physics with Artificial Satellites*. Consultants Bureau, 1965.
- [2] A. V. Gurevich, L. P. Pitaevskii, and V. V. Smirnova. Ionospheric Aerodynamics. *Space Sci. Rev.*, 9:805–+, 1969.

- [3] E. C. Whipple. *The equilibrium potential of a body in the upper atmosphere and in interplanetary space*. PhD thesis, George Washington University, 1965.
- [4] L. Kraus and K. W. Watson. Plasma motions induced by satellites in the ionosphere. *Phys. Fluids*, 1:480–488, 1958.
- [5] S. Rand. Wake of a satellite traversing the ionosphere. *Phys. Fluids*, 3:588–599, 1960.
- [6] S. D. Hester and A. A. Sonin. Laboratory study of the wakes of small cylinders under ionospheric satellite conditions. *Phys. Fluids*, 13:641–648, 1970.
- [7] U. Isensee. Plasma disturbances caused by the Helios spacecraft in the solar wind. *J. Geophys.*, 42:581–589, 1977.
- [8] U. Isensee and H. Maassberg. Particle-in-cell simulation of the plasma environment of a spacecraft in the solar wind. *Adv. Space Res.*, 1:413–416, 1981.
- [9] N. Singh and V. S. Chagani. Electron collection by a highly positive satellite in the ionosphere: test particle simulation. *J. Geophys. Res.*, 99:469–478, 1994.
- [10] N. Singh, W. C. Leung, and B. I. Vashi. Potential structure near a probe in a flowing magnetoplasma and current collection. *J. Geophys. Res.*, 102:195–208, 1997.
- [11] I. V. Rylina, L. V. Zynin, S. A. Grigoriev, and M. V. Veselov. Hydrodynamic approach to modeling the thermal plasma distribution around a moving charged satellite. *Cosmic Research*, 40:367–377, 2002.
- [12] L. Zinin, S. Grigoriev, and I. Rylina. The models of electric field distributions near satellite. In M. A. Geller, L. M. Zelenyi and J. H. Allen, editors, *Auroral phenomena and solar-terrestrial relations: Proceedings of the conference in memory of Yuri Galperin*, pages 76–83. CAWSES Handbook-001, 2004.
- [13] J.-F. Roussel and J.-J. Berthelier. A study of electrical charging of the Rosetta orbiter: 1. numerical model. *J. Geophys. Res.*, 109:A01104, doi:10.1029/2003JA009836, 2004.
- [14] A. Pedersen. Solar wind and magnetosphere plasma diagnostics by spacecraft electrostatic potential measurements. *Ann. Geophysicae*, 13:118–129, 1995.
- [15] A. I. Eriksson, M. André, B. Klecker, H. Laakso, P.-A. Lindqvist, F. Mozer, G. Paschmann, A. Pedersen, J. Quinn, R. Torbert, K. Torkar, and H. Vaith. Electric field measurements on Cluster: comparing the double-probe and electron drift techniques. *Ann. Geophysicae*, 24:275–289, 2006.
- [16] E. Engwall, A. I. Eriksson, and J. Forest. Wake formation behind positively charged spacecraft in flowing tenuous plasmas. *Phys. Plasmas*, 13:062904, 2006.
- [17] A. I. Eriksson, E. Engwall, R. Prakash, L. Daldorff, R. Torbert, I. Dandouras, and K. Torkar. Making use of spacecraft-plasma interactions: determining tenuous plasma winds from wake observations and numerical simulations. In *Proceedings of the 10th Spacecraft Charging Technology Conference (SCTC-10)*, 2007.
- [18] G. Gustafsson, R. Boström, B. Holback, G. Holmgren, A. Lundgren, K. Stasiewicz, L. Ahlén, F. S. Mozer, D. Pankow, P. Harvey, P. Berg, R. Ulrich, A. Pedersen, R. Schmidt, A. Butler, A. W. C. Fransen, D. Klinge, M. Thomsen, C.-G. Fälthammar, P.-A. Lindqvist, S. Christenson, J. Holtet, B. Lybekk, T. A. Sten, P. Tanskanen, K. Lappalainen, and J. Wygant. The electric field and wave experiment for the Cluster mission. *Space. Sci. Rev.*, 79:137–156, 1997.
- [19] A. Pedersen, F. Mozer, and G. Gustafsson. Electric field measurements in a tenuous plasma with spherical double probes. In J. Borovsky, R. Pfaff, and D. Young, editors, *Measurement Techniques in Space Plasmas: Fields (AGU Geophysical Monograph 103)*, pages 1–12. American Geophysical Union, 1998.

- [20] C. P. Escoubet, M. Fehringer, and M. Goldstein. The Cluster mission. *Ann. Geophysicae*, 19:1197–1200, 2001.
- [21] H. Rème et al. First multispacecraft ion measurements in and near the Earth’s magnetosphere with the identical Cluster ion spectrometry (CIS) experiment. *Ann. Geophysicae*, 19:1303–1354, 2001.
- [22] K. Amano, K. Tsuruda, H. Hayakawa, A. Matsuoka, and T.K. Nakamura. Interpretation of pulse-like electric field distortions observed by Exos D satellite. *J. Geophys. Res.*, 103:11851–11861, 1998.
- [23] A. Hilgers, B. Holback, G. Holmgren, and R. Boström. Probe measurements of low plasma densities with applications to the auroral acceleration region and AKR sources. *J. Geophys. Res.*, 97:8631–8641, 1992.
- [24] A. Hilgers and B. Holback. Some aspects of satellite spin effects on spherical probe measurements in a magnetized plasma. *Geophys. Res. Lett.*, 20:347–350, 1993.
- [25] A. Hilgers. Interaction between biased sunlit electron collectors in an infinite-Debye-length magneto-plasma: Electron temperature threshold effect. *J. Geophys. Res.*, 100:5705–5713, 1995.
- [26] P.-A. Lindqvist, Y. Khotyaintsev, M. André, and A. I. Eriksson. EFW data in the Cluster active archive. In K. Fletcher, editor, *Proceedings of the Cluster and Double Star symposium: 5th anniversary of Cluster in space*, page 68.1. ESA SP-598, European Space Agency., 2006.
- [27] P. W. Daly. Users guide to the Cluster science data system. Technical Report DS-MPA-TN-0015 (<http://sci2.estec.esa.nl/cluster/csds/csds.html>), Max-Planck-Institut für Aeronomie, Lindau, Germany, 2002.
- [28] B. Thiebault, A. Hilgers, A. Masson, C. P. Escoubet, and H. Laakso. Simulation of the Cluster-spacecraft floating probe potential. *IEEE Proc. Plasma Sci.*, 34:2078–2083, doi:10.1109/TPS.2006.883407, 2006.
- [29] P.-A. Lindqvist. The potential of ISEE in different plasma environments. In *Proc. of the 17th ESLAB Symp. on Spacecraft/Plasma Interactions and their Influence on Field and Particle Measurements, Noordwijk, The Netherlands, ESA SP-198*, pages 25–33. European Space Agency, 1983.
- [30] A. C. Tribble, J. S. Pickett, N. D’Angelo, and G. B. Murphy. Plasma density, temperature and turbulence in the wake of the shuttle orbiter. *Planet. Space Sci.*, 37:1001–1010, August 1989.
- [31] G. Murphy and I. Katz. The POLAR code wake model - Comparison with in situ observations. *J. Geophys. Res.*, 94:9065–9070, July 1989.
- [32] A. I. Eriksson and E. Winkler. Photoemission current and solar EUV radiation: Cluster and TIMED observations. In *Proceedings of the 10th Spacecraft Charging Technology Conference (SCTC-10)*, 2007.
- [33] J.-F. Roussel, F. Rogier, D. Volpert, J. Forest, G. Rousseau, and A. Hilgers. Spacecraft plasma interaction software (SPIS): Numerical solvers - methods and architecture. In *Proceedings of the 9th International Spacecraft Science Technology Conference (SCTC-9)*. Japan Aerospace Exploration Agency, 2005.
- [34] J. Forest, J.-F. Roussel, A. Hilgers, B. Thiébault, and S. Jourdain. SPIS-UI, a new integrated modelling environment for space applications. In *Proceedings of the 9th International Spacecraft Science Technology Conference (SCTC-9)*. Japan Aerospace Exploration Agency, 2005.
- [35] A. Hilgers, B. Thiébault, J.-F. Roussel, J. Forest, and E. Engwall. Test and validation of a new spacecraft plasma interaction software, SPIS. In *Proceedings of the 9th International Spacecraft Science Technology Conference (SCTC-9)*. Japan Aerospace Exploration Agency, 2005.